Effects of Increased Horizontal Resolution in a Simulation of the North Atlantic Ocean

AIKE BECKMANN, CLAUS W. BÖNING, CORNELIA KÖBERLE,* AND JÜRGEN WILLEBRAND

Institut für Meereskunde an der Universität Kiel, Kiel, Germany

(Manuscript received 6 January 1993, in final form 17 May 1993)

ABSTRACT

Global mean and eddy fields from a four-year experiment with a 1/6° × 1/5° horizontal resolution implementation of the CME North Atlantic model are presented. The time-averaged wind-driven and thermohaline circulation in the model is compared to the results of a 1/3° × 2/5° model run in very similar configuration. In general, the higher resolution results are found to confirm that the resolution of previous CME experiments is sufficient to describe many features of the large-scale circulation and water mass distribution quite well. While the increased resolution does not lead to large changes in the mean flow patterns, the variability in the model is enhanced significantly. On the other hand, however, not all aspects of the circulation have improved with resolution. The Azores Current Frontal Zone with its variability in the eastern basin is still represented very poorly. Particular attention is also directed toward the unrealistic stationary anticyclones north of Cape Hatteras and in the Gulf of Mexico.

1. Introduction

In recent years, the Community Modeling Effort (CME), utilizing a 1/3° × 2/5° horizontal resolution model of the North Atlantic Ocean between 15°S and 65°N, with 30 levels in the vertical, realistic coastline and topography, has led to the existence and availability of a variety of high-resolution model products. The experimental design, first described by Bryan and Holland (1989), is considered very successful in

(i) setting a first state-of-the-art "reference simulation" of the North Atlantic circulation,
(ii) reproducing many details of the hydrographic structure and velocity fields, and
(iii) by systematically varying selected model parameters, improving our understanding of unresolved modeling issues and physical processes.

The experiments, performed both at NCAR and at IfM Kiel (Böning et al. 1991a) clearly demonstrate the need for very high horizontal resolution to adequately simulate the mesoscale eddy field and its contribution to the energy cycle. With 1/3° resolution a level of model eddy energy consistent with observations is still not achieved in middle and high latitudes (Treguier 1992). So far, a wide spectrum of investigations have made use of the model data (e.g., Böning et al. 1991b; Didden and Schott 1992; Schott and Böning 1991; Spall 1990, 1992; Stammer and Böning 1992) or are currently under way (Böning and Herrmann 1994).

While most of the model mean currents and the variability in the equatorial Atlantic compare quite favorably with observations (Didden and Schott 1992; Schott and Böning 1991), the representation of the mean frontal structures and eddy variability associated with the North Atlantic Current (NAC) and Azores Current (AC) is still far from being satisfactory. Other deficiencies of the simulations include the flow pattern in the Gulf Stream separation area, the intensity of mean flow and fluctuations in the eastern basin (Treguier 1992; Stammer and Böning 1992), the strength of the meridional overturning and the representation of several water masses (e.g., arctic overflow and Mediterranean Water).

In some of the studies mentioned above, it was speculated or concluded that the 1/3° × 2/5° grid spacing is only marginally sufficient to represent the dynamically important mesoscale processes in the ocean, especially in the subpolar gyre (north of 50°N). These considerations led directly to the present study, focusing on the single aspect of increased horizontal resolution (and reduced horizontal friction) in the CME model framework. As a first report, this paper describes details of the initialization of the 1/6° × 1/5° model and presents the mean circulation (and its variability) of the North Atlantic Ocean obtained from averaging over four years of model data.

As noted previously about the CME (Bryan and Holland 1989), there are quite a number of details

* Current affiliation: Alfred Wegener Institut, Bremerhaven, Germany.

Corresponding author address: Dr. Aike Beckmann, Institut für Meereskunde an der Universität Kiel, Düsternbrooker Weg 20, D-24105 Kiel, Germany.

about the model that were chosen in a "traditional" and "conservative" manner, or for the sake of simplicity and easy accessibility. Although this was certainly a reasonable choice for the first reference experiment, it also directly points to uncertainties and weaknesses in our present knowledge (see below). Nevertheless, with the few exceptions being wind climatology and frictional coefficients, all parameterizations have been kept unchanged relative to the original NCAR experiment. This model version therefore focuses on one particular aspect, that is, the representation of sharp frontal features and mesoscale eddies; it is not intended to improve other known deficiencies, for example, the large-scale thermohaline circulation.

This paper is organized as follows: after a short presentation of the experimental configuration in section 2, important features of the model's time–mean circulation (both wind driven and thermohaline) are discussed in section 3. A first description of the fluctuating fields is given in section 4 and the effects of horizontal resolution on the meridional heat transport is investigated in section 5. A separate section (section 6) addresses the western boundary current structure of the CME model. Finally, section 7 offers summarizing remarks and an outlook. Further (regionally limited or process-oriented) intercomparisons between the 1/3° and 1/6° model results will be presented in forthcoming papers.

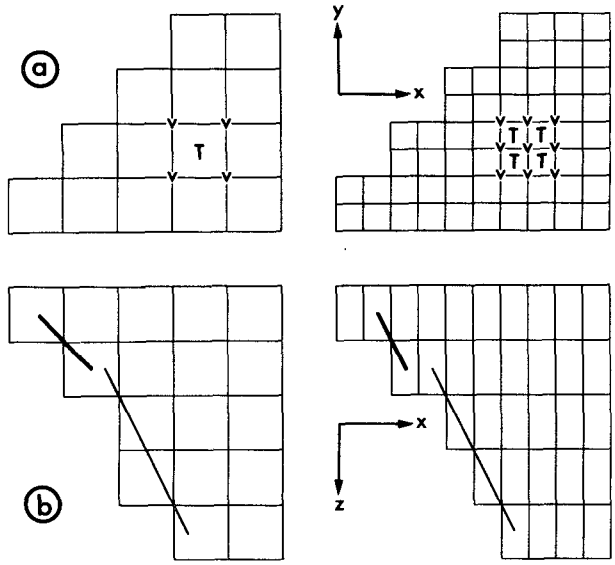

FIG. 1. (a) Horizontal arrangement of grid boxes for the 1/3° model and the 1/6° implementation; (b) topographic gradients derived for the steplike representation of water depth in the CME model of different resolution. Locally, the gradients can be larger by a factor of 2.

2. Experimental configuration

One of the important objectives in the implementation of this variant of the CME model was to guarantee continued comparability with the standard eddy resolving runs. To achieve this, changes to model formulation and parameters have been applied only very cautiously. Even where obvious deficiencies had been identified before, no corrective action was taken.

The basic idea was to exclusively change the horizontal resolution (and, subsequently the lateral diffusivity and viscosity in the model) in order to isolate the effects of those improvements on the results. The starting point was one of the 1/3° sensitivity experiments conducted at IfM Kiel. This chapter outlines several technical aspects relevant to the 1/6° implementation of the CME model.

a. Grid and topography

The finer 1/6° × 1/5° grid was constructed from the standard 1/3° × 2/5° grid by leaving the horizontal location of the velocity points on the Arakawa B grid in place and subdividing each tracer cell into four new ones (see Fig. 1a). Thus, the surface area of the two models is the same. However, the topography was specified independently for all new tracer points; as the model topography for the 1/3° × 2/5° version, it was derived from a 1/12° dataset (W. Holland 1990, personal communication). The model topography was not smoothed except for a filtering to remove all isolated single point extrema. Also, a minimum of two model levels (72 m) were specified at all ocean points. As in the 1/3° model, only the two largest Caribbean islands are treated as such, all other islands are submerged.The total volume of the two models differs by about 0.1%

Since the vertical discretization was not changed, the increase in horizontal resolution led to significant changes of local topographic slopes, a fact that was originally not intended but merely unavoidable for the model formulation. While the very steep slopes from the coarse (1/3°) grid were approximated better (see Fig. 1b), there are also many regions where the representation of the topographic slope on the 1/3° grid was already adequate with one vertical grid box per horizontal grid distance; these locations then became areas with twice the topographic slope and were found to be responsible for an increased amount of grid-scale noise in the vertical velocity and tracer fields at depth. Thus, the vertical resolution imposed limitations on the choice of the frictional parameters (see below).

b. Hydrographic data and forcing fields

In contrast to the topography, the initial fields of potential temperature θ and salinity S were derived from an instantaneous state of an experiment with 1/3° resolution (K13-4). A linear interpolation was performed for all interior points and any additional points on the boundaries were extrapolated by setting

them to the value of their nearest neighbors. The three-dimensional velocity field was initially set to zero.

In addition to earlier versions of the 1/3° model, experiment K13-4 (see Böning and Herrmann 1994) included a simple scheme for wind induced mixing following the parametrization of Camp and Elsberry (1978). The turbulent kinetic energy flux W available for entrainment at the base of the mixed layer D_m is $W = \alpha W_A e^{-D_m/D_0}$. The atmospheric flux of kinetic energy W_A is taken from the monthly values of Hellerman and Rosenstein (1983). The scale depth D_0 is taken as 50 m, and $\alpha = 0.01$. The surface boundary conditions for heat and freshwater fluxes are implemented via linear damping of model surface temperature and salinity toward an effective atmospheric temperature (according to Han 1984) and Levitus (1982) salinity climatology, respectively.

Both the 1/3° and 1/6° experiments used restoring zones of 4/3° width at the northern and southern walls where the domain was artificially closed. Within these regions, the Newtonian damping time scale varied linearly with distance from the model boundary from five to forty days (10 to 25 days for the 1/3° case). Buffer zones like these (similar ones are applied for the Mediterranean Water and over the Labrador continental shelf; see Bryan and Holland 1989) are now being widely used in basin-scale numerical modeling (e.g., Sarmiento 1986; Semtner and Chervin 1992). It had been shown in a number of sensitivity experiments with a 1° version of the model (W. Holland 1991, personal communication) that the water mass transformations taking place in the restoring areas have a strong effect on the thermohaline circulation and mean heat meridional transport. In this study, however, we are mainly interested in the structure of the upper-layer circulation and its interaction with eddies, so the exact formulation of the buffer zones is believed not to be crucial for these experiments.

c. *Course of the experiment*

For the spinup period of one year, the frictional coefficients for momentum and tracers were held fixed at the values from a 1/3° predecessor, $A_M = -0.8 \times 10^{11}$ m^4 s^{-1}, and $A_T = -2.4 \times 10^{11}$ m^4 s^{-1}. During this first year of integration, the model gradually approached and exceeded the level of kinetic energy of the 1/3° model; thereafter the friction was set to $A_M = A_T = -0.5 \times 10^{11}$ m^4 s^{-1}. A further reduction of these coefficients (which seemed desirable) was attempted but eventually rejected; it became obvious that smaller values led to an accumulation of numerical noise in the equatorial regions where the resolution of the CME model is most coarse. As a result, numerical dispersion effects were beginning to generate unrealistic water masses (see also Gerdes et al. 1991). A possible solution for this problem in future experiments would be to introduce horizontally varying coefficients in the model, tied to the local grid spacing and the regional dynamics.

A time-averaging procedure for the model analysis was initiated at the beginning of the second year, summing up the complete model state every three days, thus accumulating 488 individual fields to make up the mean. Figure 2 shows the evolution of the basin-averaged kinetic energy during the five years of integration. While the amplitude of the seasonal variation in both model versions is very similar, basically indicating the response of the tropical ocean to the seasonal forcing, the overall energy level of the higher-resolution run is increased by a factor of 1.5, giving a first indication of larger model velocities.

On a CRAY-2, the computation of the 1/6° model (6.3 million grid points, with approximately 50% being active) over one year took approximately 500 hours of CPU, for a 60 Mword core-contained model code.

3. The time-mean circulation

Any description of a high-resolution model has to remain incomplete to some degree considering the enormous amount of model data and physical/geographical situations available. The emphasis of the present study lies on a first description of global time-mean and eddy fields and comparisons with the corresponding 1/3° run. Several "standard" test regions will be examined and physically important processes will be addressed.

a. *Wind-driven circulation and vertically integrated transport*

The vertically integrated transport in the North Atlantic is expected to be relatively independent of the

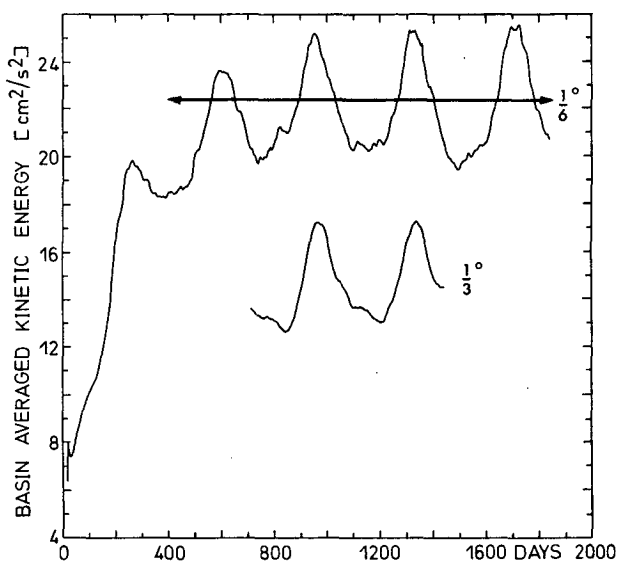

FIG. 2. Time series of the basin-integrated kinetic energy during five years of the increased resolution experiment. For comparison, the curve from the two previous years of the 1/3° calculation was added. The averaging period is also indicated.

model resolutions discussed here. The wind stress was interpolated from a 1° × 1° dataset (Isemer and Hasse 1987); therefore, no additional spatial details of the forcing fields are used for the increased resolution case. The linear Sverdrup relation gives a maximum transport of about 35 Sv (1 Sv ≡ 1×10^6 m^3 s^{-1}) at the eastern edge of the western boundary current system in the subtropical North Atlantic. Differences in time-averaged transport should only occur in regions where the local dynamics are far from being linear or where the topography has changed significantly.

The four-year mean mass transport streamfunction of the 1/6° resolution model is displayed in Fig. 3a. In accordance with the above considerations, the general impression is that differences relative to the 1/3° results (see Bryan and Holland 1989; Treguier 1992) are only of minor importance. The transport through the Gulf of Mexico reaches about 25 Sv, increasing along the path of the Gulf Stream to 40–50 Sv at Cape Hatteras; an anticyclonic cell fills most of the Mid-Atlantic Bight. This unrealistic Gulf Stream separation from the coast is common to many primitive equation model experiments and will be investigated in more detail in section 6 below. Farther downstream, the boundary current separates from the coast and shows large stationary meanders, but then "disintegrates" into a broad eastward flow, before forming another western boundary current that sets northward through Flemish Pass (the gap between Newfoundland and Flemish Cap). Here, at 50°N, the NAC is formed in the model by unification of this flow and the counterclockwise subpolar circulation (the Labrador Current). The eastward penetration of the NAC as a sharp frontal jet is limited to the area west of the Mid-Atlantic Ridge (MAR), feeding directly into the East and West Greenland Currents. In general, the 1/6° model reproduces many elements of the wind-driven circulation in very much the same way as the coarser 1/3° model runs did.

From the difference plot (1/6° − 1/3°; Fig. 3b), however, it becomes clear that local changes are substantial: the unrealistic anticyclonic cell north of Cape Hatteras has almost doubled its strength, from 45 to 90 Sv, and, even more dramatically, a similar cell has developed from 25 to 80 Sv in the Gulf of Mexico; the NAC in the 1/6° case is completely confined to Flemish Pass—the branching into flow around both sides of this topographic obstacle from the 1/3° model is no longer present in the higher-resolution run. The subpolar gyre is stronger in most areas, indicating that eddy activity and flow topography interaction must have changed with resolution. Even more pronounced than in the 1/3° run, the model favors flow concentrated along the shelf break. It is important to note that the differences tend to strengthen the preexisting flow patterns, like the Cape Hatteras cell and the Loop Current cell. The magnitude of the differences can reach 55 Sv in closed circulations along the western boundary (Fig. 3b),

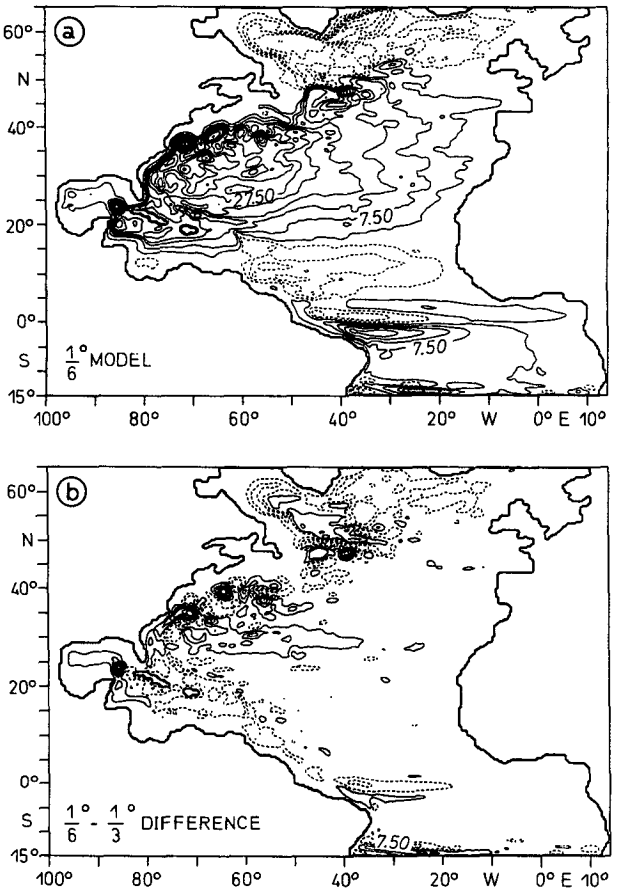

FIG. 3. (a) Four-year averaged mass transport streamfunction for the 1/6° simulation; (b) difference field 1/6° model − 1/3° model. Contour interval: 5 Sv.

while other structures like the equatorial circulation are much less influenced by the increase in resolution.

The kinetic energy of the mean flow (MKE) for a 1/3° run (N13-2) was investigated by Treguier (1992). The Kiel 4 experiment produced a very similar pattern, with values exceeding 1000 cm^2 s^{-2} being limited to the western boundary current (WBC) between 20° and 40°N and the equatorial circulation system. In both areas, the MKE has not changed very much with doubled resolution; maximum values of MKE in the Gulf Stream (including the separation anticyclone) are 7000 cm^2 s^{-2} for the coarser and 8000 cm^2 s^{-2} for the finer resolution case; maximum values of 14 000 cm^2 s^{-2} occur in the 1/6° Gulf of Mexico Loop Current anticyclone. We will return to this in section 6.

A closer look at the geographical distribution of MKE concentrates on the central North Atlantic (Fig. 4), away from those areas. With both model resolutions, the penetration of the Gulf Stream into the ocean's interior is rather limited. Although the overall level of MKE is higher in the 1/6° model, there is no indication that a significantly larger portion of it is advected eastward into the interior of the ocean.

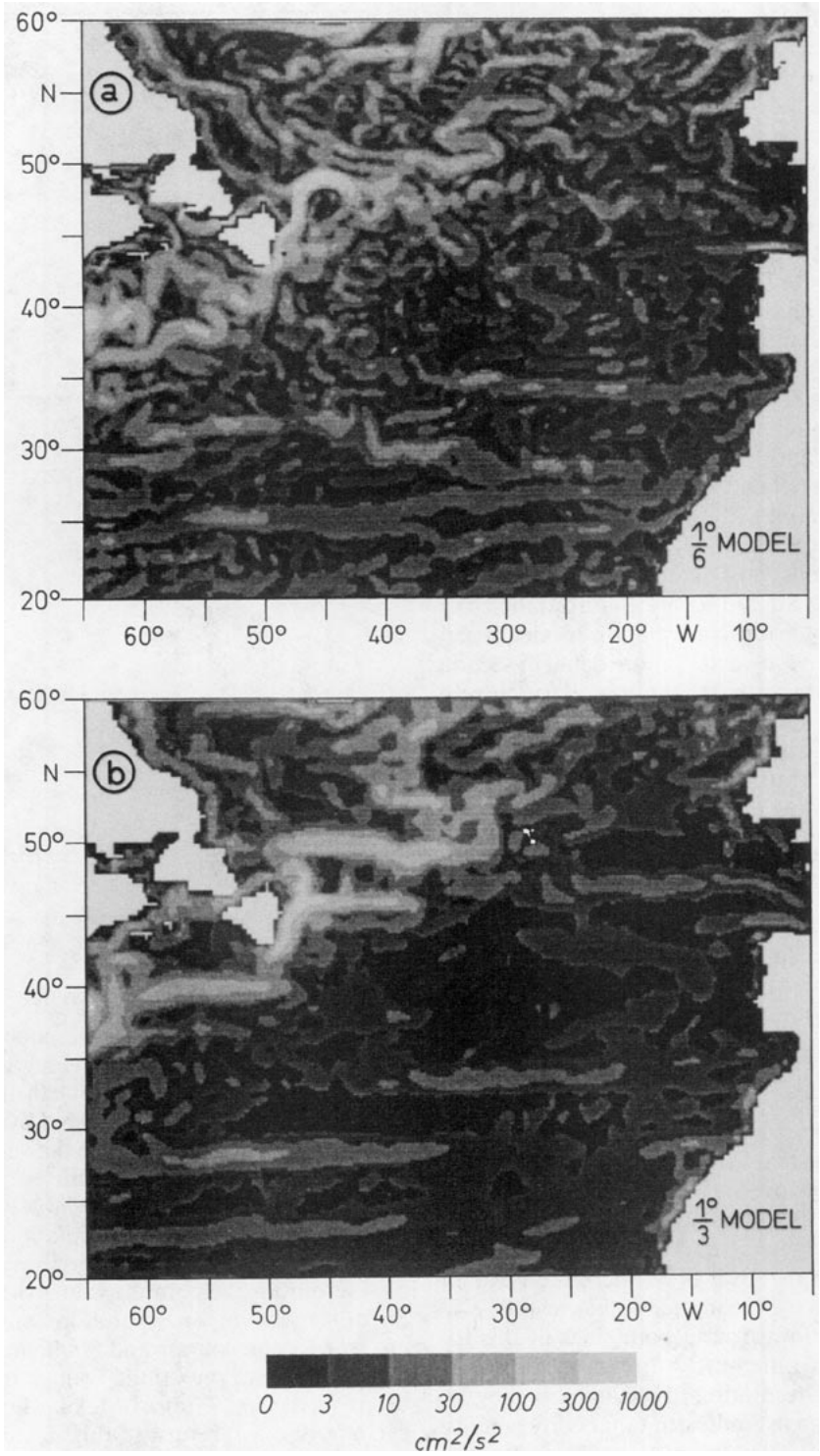

FIG. 4. Mean kinetic energy (MKE) in the central North Atlantic in 100-m depth for (a) the 1/6° model; and (b) the 1/3° model.

The occurrence of mainly zonal bands of increased MKE in the open ocean in both model resolutions (but with increased intensity in the 1/6° model) is the dominant feature in the central and eastern subtropical gyre. Their exact location differs by a few degrees latitude with changing model resolution. Most of those struc-

tures cannot be related to observed phenomena; some of them in the 1/6° model, however, seem to be tied to topographic features, like the Atlantis Fracture Zone at 30°N, 42.5°W and the Maxwell Fracture Zone at 47.5°N, 27°W. Similar concentrated bands of zonal time-mean flow in numerical experiments have been reported by Cox (1987). The underlying dynamical processes are not completely understood; their meridional scale of 100–200 km is consistent with both low-frequency waves radiating from unstable regions of westward flow in the southern subtropical gyre (see Spall 1992, 1993) and mean flow generation by the mesoscale variability, a manifestation of the energy cascade in quasi-homogeneous turbulence.

Relative to the 1/3° model the MKE of the 1/6° run is generally increased by a factor of 2 for the "background" energy and up to a factor of 1.5 for jet regions. Still, the subtropical gyre east of the MAR is far too "quiet" as compared to observations (e.g., Krauss and Käse 1984). The eastward AC at 35°N and the equatorward Portugal Current (PC) are clearly underrepresented. Two regions of the North Atlantic Ocean are chosen here to demonstrate the ability (or lack thereof) of the CME model to reproduce the observed surface flow patterns: the western boundary current system (Fig. 5a) and the more "quiet" Canary Basin in the northeast Atlantic (Fig. 5b).

Originating with 25 Sv in the Gulf of Mexico, the model Gulf Stream stays close to the shelf break between Florida and 40°N, setting up an enormous recirculation cell in the Mid-Atlantic Bight (see section 6 for a more detailed discussion). The connection with the NAC is somewhat obscure, since the jet stream loses its integrity at 55°W. A series of wavelike jets fills the North Atlantic between 65° and 50°W. A more defined current is reestablished in the Grand Banks region where the Labrador Current should flow southward along the continental slope (Greenberg and Petrie 1988). In the 1/6° model, however, the flow through Flemish Pass is entirely northward, joining the Labrador Current north of Flemish Cap to form a main front at about 50°N. Again, the model boundary current seems unable to separate properly from the coast. Maximum velocities at 100-m depth are found to be 150 cm s^{-1}; however, these values are not occurring in the proper Gulf Stream but in the Cape Hatteras anticyclone.

On the eastern side of the basin we find various current branches with O(10) cm s^{-1} mean flow. One may attempt to identify observed current bands as proposed by Krauss (1986): at 46°N a branch that had separated from the NAC continues zonally to reach into the Bay of Biscay, then turning southward as a PC. Another zonal flow band can be found in 34°N, somewhat to the south of the observed latitude of the AC. However, there is no obvious connection to the NAC source region at Newfoundland and the velocities are an order of magnitude too weak to be a realistic representation of the Azores Front. We have to conclude that important dynamical properties of the circulation responsible for the real Azores Current Frontal Zone (ACFZ) are not represented adequately in the present model. The ACFZ is considered to be a major source of variability in the eastern basin, and the implications of the weak AC regime on the eddy kinetic energy level in this region will be investigated in more detail in section 4.

b. Meridional overturning and thermohaline circulation

It seems useful to begin the examination of the thermohaline circulation in the model with the inspection of the basinwide zonally integrated meridional overturning (Fig. 6). (It is important to emphasize here that none of these experiments have been carried out to thermodynamic equilibrium and that, consequently, conclusions on the final strength and pattern of the thermohaline circulation cannot be drawn.) In the vertical, the three well-known overturning cells can be identified: the relatively shallow (200–300 m deep) wind-induced Ekman cells, the North Atlantic Deep Water (NADW) cell in the upper ocean, mainly driven by downwelling in the north, and the deep Antarctic Bottom Water (AABW) cell below.

While the Ekman and bottom water cells in the finer resolution model are slightly enhanced in size and strength, the rate of meridional overturning in the NADW cell is found to decrease with increasing model resolution: the maximum transport of the 1/3° case is 12 Sv, for the 1/6° case only 9 Sv. At the same time, the lower boundary of the cell is shifted upward from 2500 to 2250-m depth. Interestingly, this tendency also persists for even coarser horizontal resolution; for example, the maximum transport of a coarse (1° × 6/5°) resolution experiment with the same forcing, geometry, and topography (R. Döscher 1991, personal communication) is 16 Sv. The non–eddy resolving experiment therefore appears to be much closer to estimates from observations, which give values of about 17 ± 5 Sv in the subtropical North Atlantic (see Hall and Bryden 1982; Roemmich and Wunsch 1985).

Attempts to explain these model results have to address some of the incompletely known sensitivities of this type of numerical simulation. Besides resolution and friction, the choice of other parameters may be crucial to the resulting circulation as well. First, we are faced with the fundamental difficulty to exclusively change the resolution of a numerical model. For instance, it is conceivable [judged from 1° model experiments by W. Holland (1991, personal communication)] that the efficiency of the restoring zones determine the amount and maximum depth of the downwelling to a significant extent; since its efficiency is determined both by the damping time scales, the number of points, and by the physical width of the layer, the northern boundary condition in both model

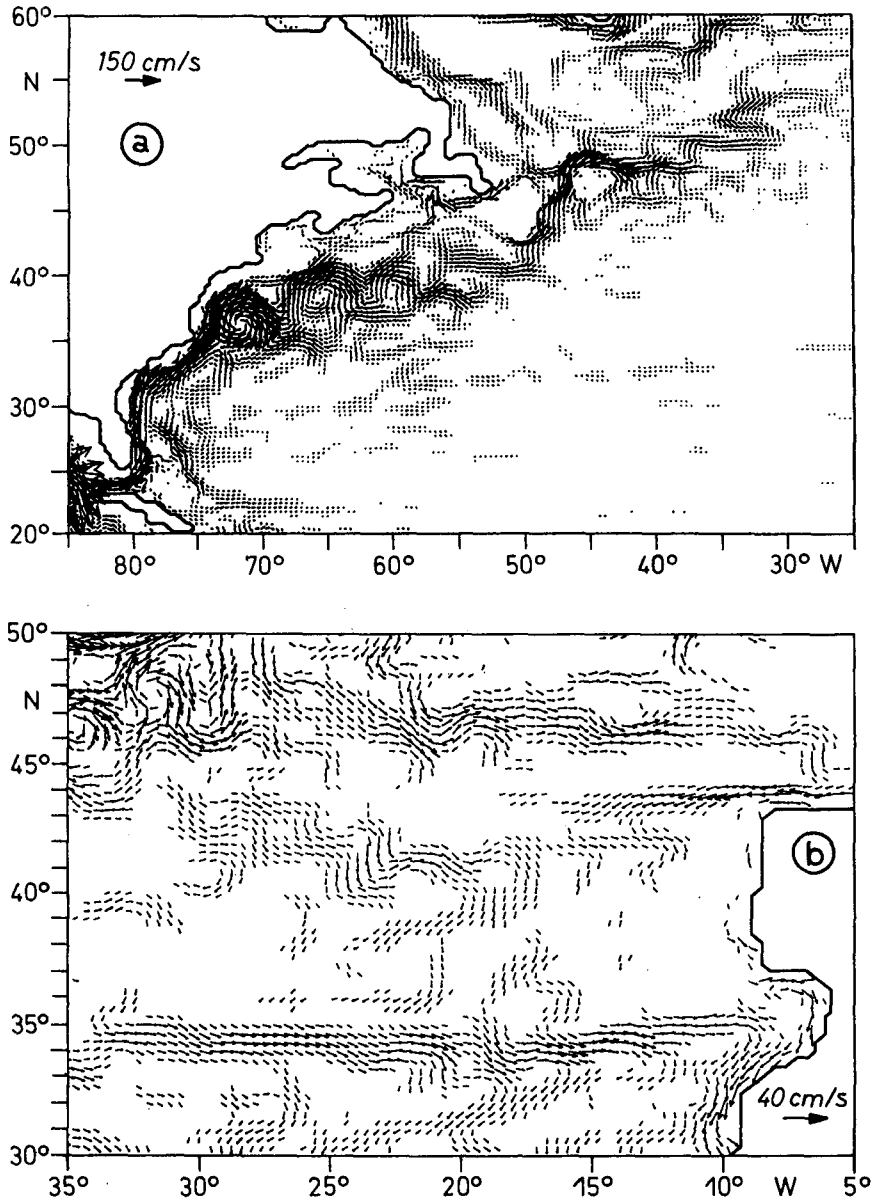

FIG. 5. Horizontal mean velocities in 100-m depth (a) in the northwest Atlantic, featuring the Gulf Stream and the North Atlantic Current, maximum vector length: 150 cm s^{-1}; (b) in the Canary Basin, maximum vector length: 20 cm s^{-1}.

versions (eight points for the 1/6° and four points for the 1/3° experiment) cannot be considered identical even though both span the same physical distance.

It is also obvious from the figures that the model AABW cell extends too far north. This can be attributed to the fact that the lower NADW is not properly prescribed in the northern restoring zone where the hydrographic fields are "nudged" toward monthly mean climatology. While the upper core of the NADW [flowing southward along the western boundary as a deep western boundary current (DWBC)] has a clear signature in the zonally integrated field in lower and midlatitudes (at depths around 2000 m), the lower core is missing completely from the models. This, of course, is true irrespective of horizontal resolution. Recent experiments with 1° and 1/3° models (Döscher et al. 1993) show that the water masses specified as the northern boundary condition do have a large influence on the strength of the overturning: an improved representation of the overflow water masses leads to increased transports. The presented results might therefore be explained by the strong sensitivity of the thermohaline circulation in the model on details of the implementation of the northern boundary condition.

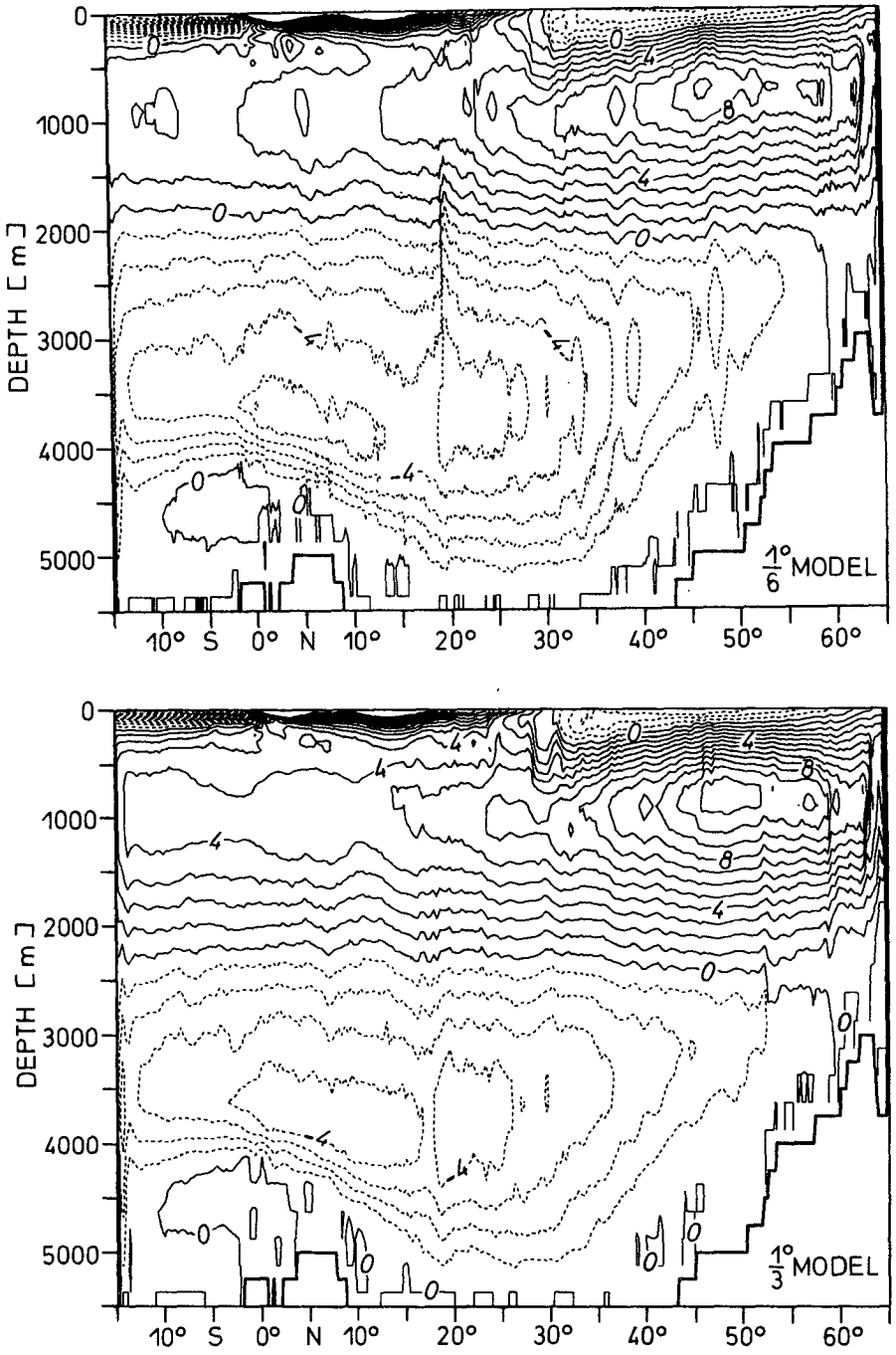

FIG. 6. Zonally integrated meridional mass transport for (a) the 1/6° model; and (b) the 1/3° model. Contour interval: 1 Sv. Note that the isolated "fault" at 19°N in the overturning streamfunction of the 1/6° model is related to extremely large vertical velocities at the flanks of the Puerto Rico Trench, not present in this magnitude in the standard resolution CME model.

This implies that conclusions about the effect of the higher resolution in the model's interior should be drawn with caution.

As a quantitative example of the combined thermohaline and wind-driven components of the flow in the model, the meridional transport balance along a zonal section at 25°N is considered next (Fig. 7). In this simple schematic diagram the Sverdrup regime was assumed to extend from the eastern boundary to 72.5°W and down to 1000-m depth. The western

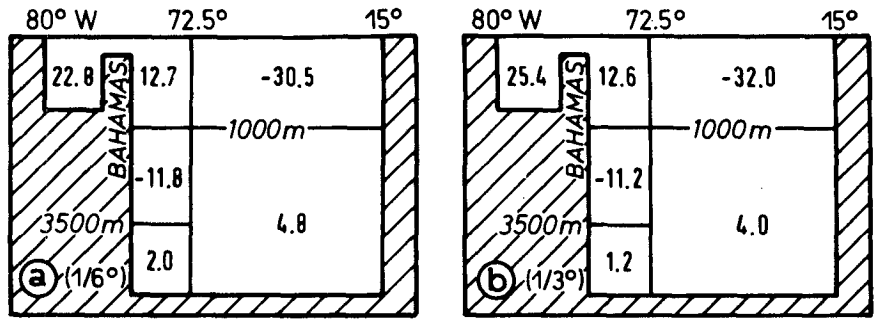

FIG. 7. Schematic diagram of the meridional transport across a zonal section at 25°N for (a) the 1/6° model and (b) the 1/3° model. Transports are in Sverdrups.

boundary current system in the model is subdivided into four members, based on the above considerations: the Florida Current between Florida and the Bahamas, the Antilles Current in the upper 1000 m east of the Bahamas, the southward DWBC in the interior, and a northward deep flow below 3500 m. In general, both models give a very similar picture. The differences are small enough to be attributed to the specific choice of regime boundaries, whose exact location is arbitrary to some degree. The only exception is the transport through the Florida Straits, which is completely confined by topography. Its time-mean amplitude is reduced from 25.4 Sv in the K13-4 run to 22.8 Sv in the higher-resolution experiment. This may be interpreted as the result of the larger variability due to the reduced friction (see Böning et al. 1991a), which tends to diminish the net transport. The resulting 10% change is comparable in magnitude to differences produced by different wind products (see Böning et al. 1991b).

On the other hand, both model resolutions give a much smaller northward transport than the 30.5 Sv of the purely wind driven model of Anderson and Corry (1985). A more detailed analysis shows that model results intimately depend on the degree of realism in the representation of the complicated topographical situation in the western Atlantic. For example, the flow through the passage between Cuba and the Bahamas is negligible in the CME calculations, in accordance with recent observations by Schmitz and Richardson (1991) but in contrast to the Anderson–Corry model where the coarser resolution introduces artificially wide and deep passages.

To obtain an idea of the total northward transport the Antilles Current east of the Bahamas has to be taken into account. Combined, the upper-ocean northward transport in the 1/6° model yields about 35.5 Sv, distinctively less than the 38.0 Sv of the corresponding 1/3° run. Thus, the total transport of the WBC seems to be in better agreement with estimates from observations, that is with the sum of 30–32 Sv of northward transport for the Florida Current (e.g., Schott et al. 1988) and the about 4 Sv for the Antilles Current (Olson et al. 1984).

Applying our present knowledge of the thermohaline component at this latitude [17 Sv basinwide by Roemmich and Wunsch (1985) and 13 Sv for the thermohaline contribution to the transport through the Florida Straits by Schmitz and Richardson (1991)]; however, the 5–6 Sv at 25°N in both models must be seen as a severe underestimation of the overturning. It seems quite possible that a more realistic meridional overturning will increase the strength of the Florida/Antilles Current system by another 6 Sv, again farther away from observations. This would indicate that the mean wind stress curl of the Isemer–Hasse climatology for the subtropical North Atlantic is too strong. This line of arguments, however, does not take into account any nonlinear effects caused by an altered thermohaline circulation.

4. Eddy variability

The most important reason for conducting a higher horizontal resolution experiment in the CME configuration was the expected increase of eddy energy to a more realistic level, which is needed to assess the role of the variability in the general circulation. For the present study, all deviations from the 4-year mean are included in the term "eddy variability"; that is, interannual, seasonal, and all high frequency fluctuations are not considered separately.

A horizontal map of eddy kinetic energy (EKE) in the near-surface levels (100 m) of the model is displayed in Fig. 8, again for both the 1/6° and the 1/3° case. From the figures, three differences are immediately visible: in the higher-resolution case the maximum values close to the western boundary are higher by a factor of three, regions of high variability are larger, and the eastern basin is much more energetic than in the 1/3° run. This general result is especially true for the regions north of 50°N, where patches of increased EKE now exist from boundary to boundary. Most of the centers of eddy activity in the fine-resolution case are closely related to the regions of enhanced mean flow (cf. Fig. 4). These fluctuations can be explained as meandering or weak instabilities of the background flow. In many places,

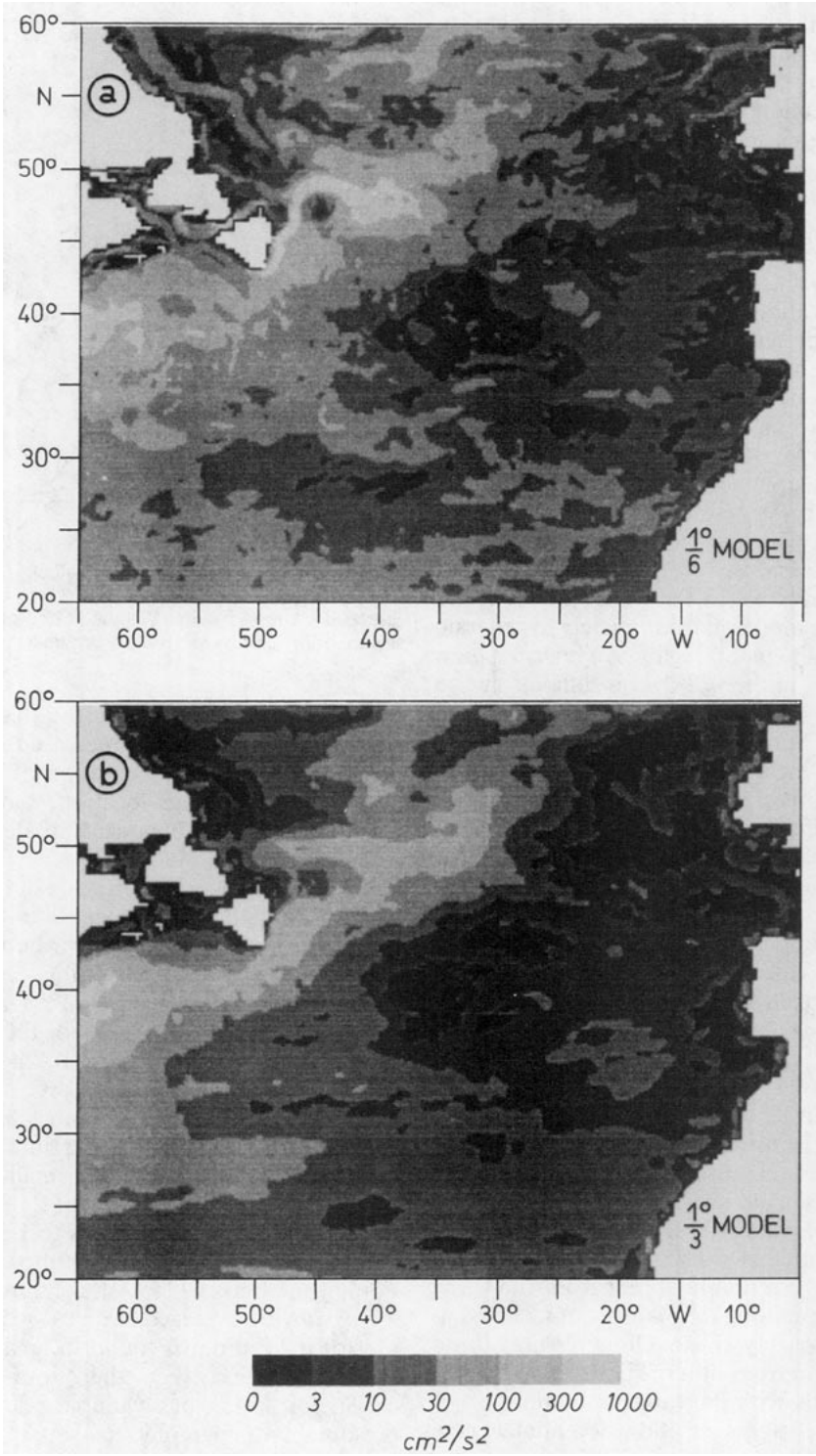

FIG. 8. Eddy kinetic energy (EKE) in the central North Atlantic in 100-m depth for (a) the 1/6° model and (b) the 1/3° model.

the MAR represents a region of reduced variability. Exceptions are those fracture zones, where the resolution is fine enough to allow for an appreciable mean flow to cross the ridge. However, despite the overall increase, the level of EKE is still not satisfactory in many regions of the 1/6° model.

A meridional section of the upper-ocean variability (values from 100-m depth of the model were taken as representative) along 30°W is presented to illustrate this (Fig. 9). The section was chosen because it is undisturbed by continents and should exhibit three major bands of variability, well known from field studies: the NEC, the AC, and the NAC. Added to the figure as a reference are the most recent results from the surface drifting buoy dataset obtained by IfM Kiel over the past ten years (Krauss and Käse 1984; B. Brügge 1992, personal communication). The buoys are drogued in 100 m; data from buoys with lost drogues are eliminated according to the procedure described by Brügge and Dengg (1991). Both the buoy and model EKE values are zonally averaged from 25°W to 35°W and over one degree in meridional direction. In general, the 1/6° model has a larger and therefore more realistic EKE level than the lower-resolution case; remarkably, the peak associated with the NAC is almost doubled in amplitude. The signature of a fluctuating AC, however, is hardly identifiable in the EKE field of either model version; both models fail completely to generate the observed variability in this region. An interpretation of the peak at 60°N in the 1/6° data is difficult due to the close proximity of the northern boundary layer.

Recent results of Stammer and Böning (1992) confirm the idea that a linear relationship between the first internal Rossby radius of deformation R_i and the eddy length scales L exists in the North Atlantic. Consequently, it seems plausible that for a successful simulation of the eddy field and the observed level of EKE in a numerical model, the local horizontal scale $2\pi R_i$ has to be resolved properly (i.e., by at least several grid points). Accepting this view, and assuming that six grid points per wavelength represent a sufficiently accurate approximation, realistic EKE values can be expected equatorward of 28° and 42°N for the 1/3° and 1/6° model, respectively. The 1/6° results show that both increase and overall level of EKE is higher north of 50°N rather than in midlatitudes between 30° and 40°N. This indicates that resolution alone, while necessary, is not sufficient to successfully model the observed variability patterns and levels. With the ACFZ as an important source of baroclinic instability in the eastern basin being essentially absent from the CME models, the only remaining mechanisms for EKE generation are the monthly mean climatological wind forcing and radiation from other regions. This has not changed significantly with increased resolution.

The horizontal patterns of eddy potential energy (EPE, not shown) inferred from the distribution of T_{rms} in the upper ocean is very similar to the corresponding field of the 1/3° model. Especially in the eastern basin, the increased near-surface EKE does not go hand in hand with a more variable temperature field, thus indicating that the reservoir of mean available potential energy is not accessed by more vigorous and/or more frequent baroclinic instability processes. Close to Newfoundland, at 50°N, where the maximum values of EKE appear, the EPE is increased significantly, now reaching the level of observations. Unfortunately, this occurs at the "wrong" location, that is, northwest instead of east of the Flemish Cap along the main path of the model mean flow.

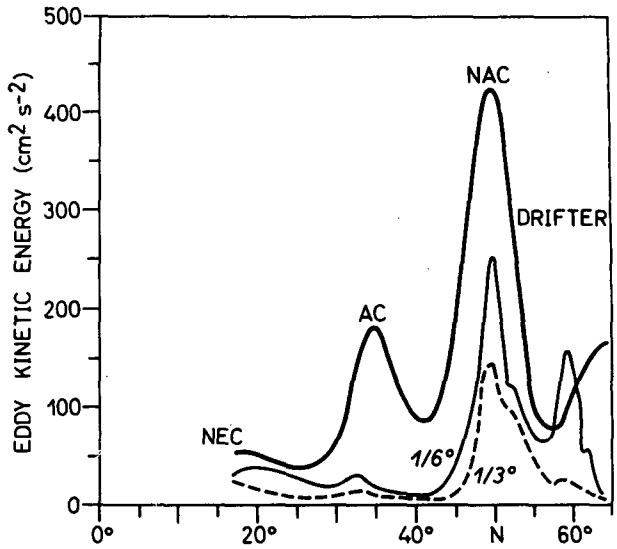

FIG. 9. Meridional section of EKE along 30°W (averaged zonally over ten degrees from 25°W to 35°W and meridionally over one degree) for the 1/6° and 1/3° models and observations from IfM surface drifting buoys (B. Brügge, personal communication).

The vertical penetration scale of the increased variability is limited to the upper 1000–1200 m. Figure 10 shows the typical vertical distribution of MKE and EKE for both model resolutions in several different dynamical regimes: a 3° × 3° average of the Gulf Stream area (including parts of the adjacent western subtropical gyre), and 10° × 10° boxes in the central eastern basin, the NEC and NAC areas. Despite large differences in the absolute value of mean and eddy energies all subdomains show a similar relative increase for doubled resolution, fairly small for the mean but significant (roughly a factor of 2) for the eddy component. This tendency seems to be universally valid [see also results from the box model experiments by Böning and Budich (1992)]; the same increase is found for basinwide-averaged profiles. An increase in EKE toward the bottom is found in areas with large topographic variations (e.g., the Azores region), an indication for strong but variable bottom-trapped flow, presumably topographic Rossby waves.

A more detailed intercomparison between the upper-ocean model variability and observed fields from surface drifters and satellite altimetry will be presented in a separate study by Beckmann et al. (1993).

5. Meridional heat transport

Overturning in the meridional–depth plane is a key mechanism for the meridional transport of heat. Both

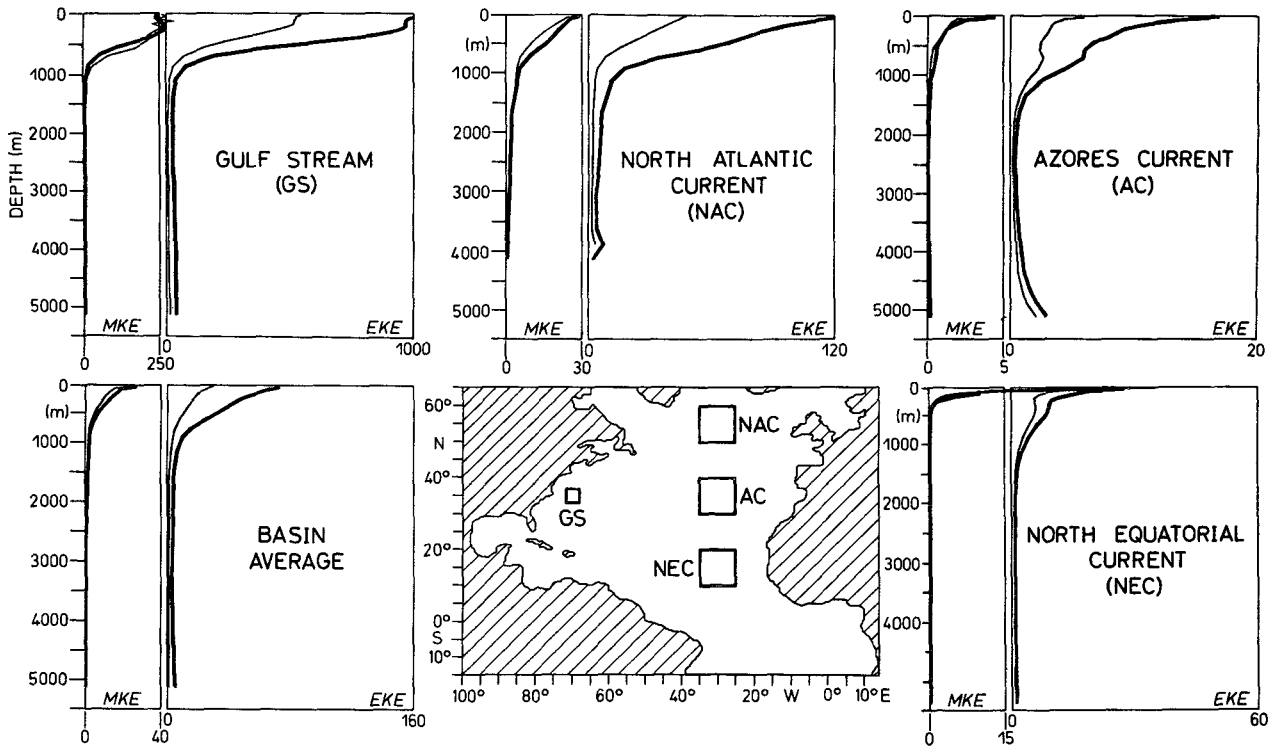

FIG. 10. Vertical profiles of mean and eddy kinetic energy, for both the 1/6° and the 1/3° model, representative of four dynamically different geographical regions and the domainwide average. Thin (fat) lines represent data from the 1/3° (1/6°) model.

thermohaline and Ekman cells contribute to the observed midlatitude maximum of the northward heat flux of 1.2 PW (Hall and Bryden 1982). Figure 11 shows the net (zonally and vertically integrated) heat transport for both model resolutions, and its decomposition into mean and fluctuating component. The total transport curves from both models have a very similar shape, with negative heat transport (directed southward into the buffer zone) south of the equator. This can be explained by the fact that the net meridional heat transport in that area is given by a delicate balance between northward transport due to the deeper NADW cell, and the southward transport due to the shallow, wind-driven overturning cell in the upper 200 m. A 1/3° sensitivity study performed in Kiel has shown a strong dependence of the net meridional transport in the equatorial Atlantic on details of the mixed-layer formulation as well as the southern sponge layer. For example, experiments K13-1, 2 and 3 without a mixed layer have a positive (poleward) heat transport throughout the domain. Again, this result points to relatively unexplored sensitivities in connection with common parametrization approaches.

North of the equator, the overall shape of the total heat transport curve and the maximum values in both cases are also very close ($HT = \rho_0 c_p \int\int \overline{v\theta}\, a \cos\phi d\lambda dz$ = 0.68 PW and 0.65 PW, respectively, at 36°N). This fact, in connection with the reduced time-mean meridional overturning (see section 3 and Fig. 6) raises the question about the role of the eddy heat flux ($EHT = \rho_0 c_p \int\int \overline{v'\theta'}\, a \cos\phi d\lambda dz$) and the obvious compensation by a transport of the mean flow field ($MHT = \rho_0 c_p \int\int \bar{v}\bar{\theta}\, a \cos\phi d\lambda dz$) of opposite sign. This result, the "no additional net heat transport by eddies," is not completely unexpected, since it has been reported from numerical experiments before (Cox 1985; Böning and Budich 1992). In a hierarchy of single state variable models (effects of salinity on density neglected) with increasing resolution the net poleward heat transport was insensitive to the presence of eddies; that is, there was a compensation between the meridional eddy flux of heat and the additional flux by eddy-induced mean flow (Bryan 1991); recently the same result was found for an isopycnic coordinate model (Drijfhout 1994). As was pointed out by Bryan (1986), to the extent that eddy trajectories are largely excursions on isopycnal surfaces, a net eddy heat transport requires the existence of temperature gradients on those surfaces, which was not the case in the idealized models. Our results indicate, however, that the inclusion of salinity does not significantly enhance the heat transport by eddies to alter the general picture.

In both model resolutions, the eddy part of the heat transport is negative between the equator and 34°N and positive poleward of this region. The typical magnitude of 0.1–0.2 PW for the EHT has not changed

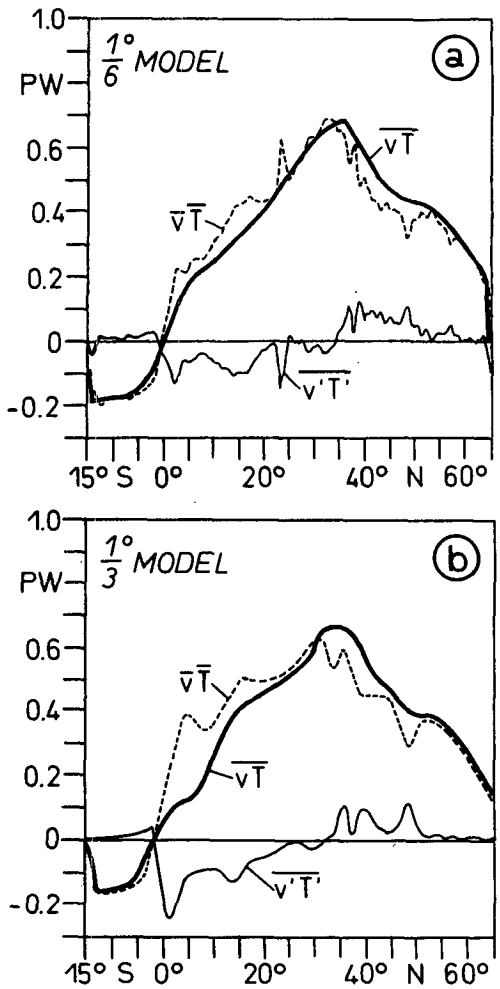

FIG. 11. Zonally and vertically integrated meridional heat transport decomposed into mean and eddy components for (a) the 1/6° model and (b) the 1/3° model.

with resolution either; there are, however, increased transports north of 50°N, the area that is believed to have gained most from the increase in resolution. This result is in contrast to the box model results by Böning and Budich (1992), who find a more general increase in EHT with resolution. One reason might be that the main fronts in the North Atlantic model are not predominantly zonal, such that a cross frontal eddy heat transport does not coincide with a meridional heat transport, and that the penetration of the NAC in both CME model versions is still too small. Note that the effects of the unrealistically strong anticyclones are clearly visible in the eddy heat transport (at 23° and 37°N). Due to their sheer strength, even relatively small fluctuations in amplitude and position can and do lead to a significant heat transport. Those peaks have to be considered as spurious.

A complete investigation of the eddy heat transport issue is beyond the scope of this paper but some facts may contribute to the discussion: Although it appears (from Fig. 11) that the change in net meridional heat transport introduced by the eddy activity is a small fraction of the total, which could be balanced by a modified surface heat flux, this might not be the case. To get an idea of the horizontal distribution of EHT the divergence of the vertically integrated heat transport $(\rho_0 c_p/(a\cos\phi)\int(u\theta)\lambda + (v\theta\cos\phi)_\phi dz)$ was calculated and decomposed into its mean and eddy part. A map of this quantity (not shown) reveals that the significant contributions from eddy heat flux are limited to very few relatively small regions in connection with the western boundary current. There, the heat flux divergence introduced locally by the eddy terms can reach up to 10 000 W m^{-2} and therefore cannot be balanced by the surface Newtonian restoring term (which would require hundreds of degrees difference between the surface and equivalent atmospheric temperature). Consequently, it has to be balanced by the mean flux divergence, such that the actual eddy contribution is limited to one that can be locally compensated by the eddy-induced changes in mean transport. This may explain the general tendency toward decreased overturning with increasing resolution and eddy activity. The predominantly local character of the eddy fluxes are also responsible the nonsmoothness in the meridional overturning streamfunction (see Fig. 6).

Regardless of what the reasons are, the results obtained point to the conclusion that the effect of eddies on the net meridional heat transport in this kind of numerical models is very small. But as long as no feedback from an active atmosphere and Arctic Ocean is allowed, the relative contributions of mean and fluctuating part of the meridional heat transport cannot be quantified.

6. Western boundary current structure

The (optically and, in part, dynamically) dominating features of the model runs are the anticyclones in the Mid-Atlantic Bight [the Cape Hatteras cell (CHC)] and in the Gulf of Mexico [the Loop Current cell (LCC)]; they deserve a more detailed description. This subsection will compile several aspects of the occurrence and maintenance of strong anticyclones in models of the CME type, although no conclusive explanation can be given at this time. One important question to ask is whether the anticyclones at both ends of the WBC are the *result* or the *cause* of particular model deficiencies.

a. How does the Gulf Stream look prior to separation?

The mean boundary current axis is determined from the position of the maximum mean kinetic energy (Fig. 12) in 100-m depth. (The often referred to classical definition of the 15°C isotherm in 200 m lies right

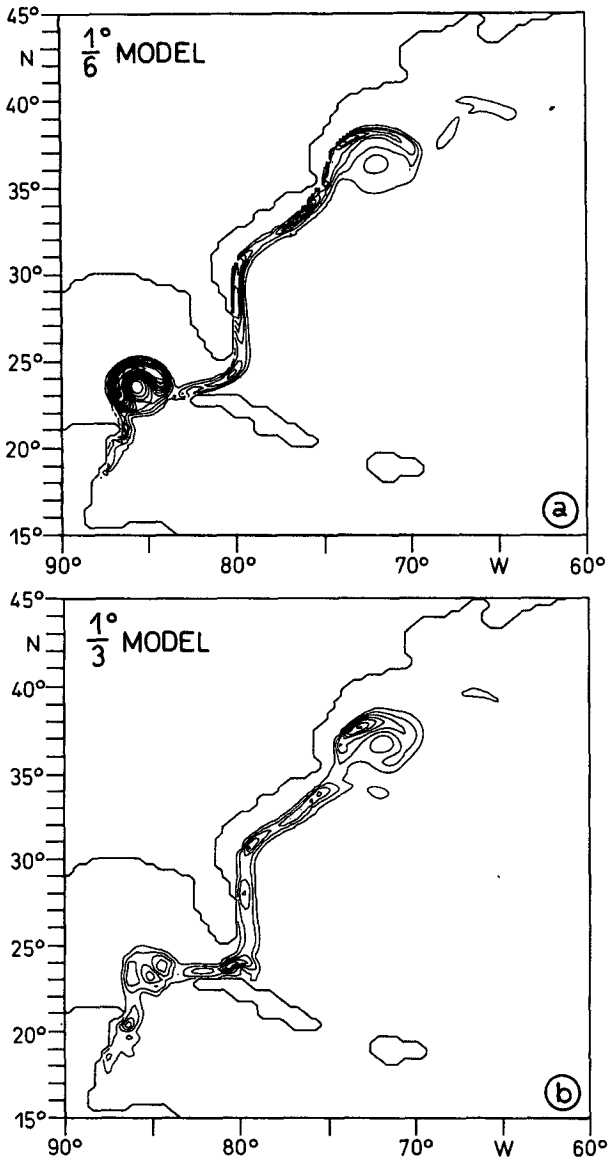

FIG. 12. Mean kinetic energy for the western boundary current system, indicating the axis of the boundary current: for (a) the 1/6° model and (b) the 1/3° model. Contour interval: 1000 $cm^2 s^{-2}$.

along the shelf break front and is therefore not very illustrative here. This indicates again the fact that the model Gulf Stream is by far too close to the coast everywhere.) For comparison, the 1/3° results are also presented. It is quite obvious that the mean path in both model resolutions looks reasonable from the Gulf of Mexico to Cape Hatteras, where the jet curvature begins to deviate from the observed. While in reality the Gulf Stream continues on a straight path at 35°N (thus turning away from the continent), it bends toward the coast in the model, falling into the strong anticyclone. Cross sections of the alongjet velocity through the current (Fig. 13) exhibit that the maximum flow velocities are shifted offshore with depth, a characteristic of the real Gulf Stream as well. It is obvious from these figures that the boundary current leans against the topography all the way from Florida to Cape Hatteras, with the maximum located above the shelf break. The secondary circulation (normal to the jet) maintains constant upwelling along the continental slope, thus creating a strong shelf break front. Leaman et al. (1989) report Gulf Stream velocities of 160–190 cm s^{-1} in the long-term mean. While maximum time-mean surface velocities in the model are found in the LCC (163 cm s^{-1}) the boundary current only reaches 113 cm s^{-1}, before "disappearing" at 70°W in currents of less than 40 cm s^{-1}. The maximum velocity is too small by a factor of 1.5 and this has not changed significantly with increasing resolution. In addition, the

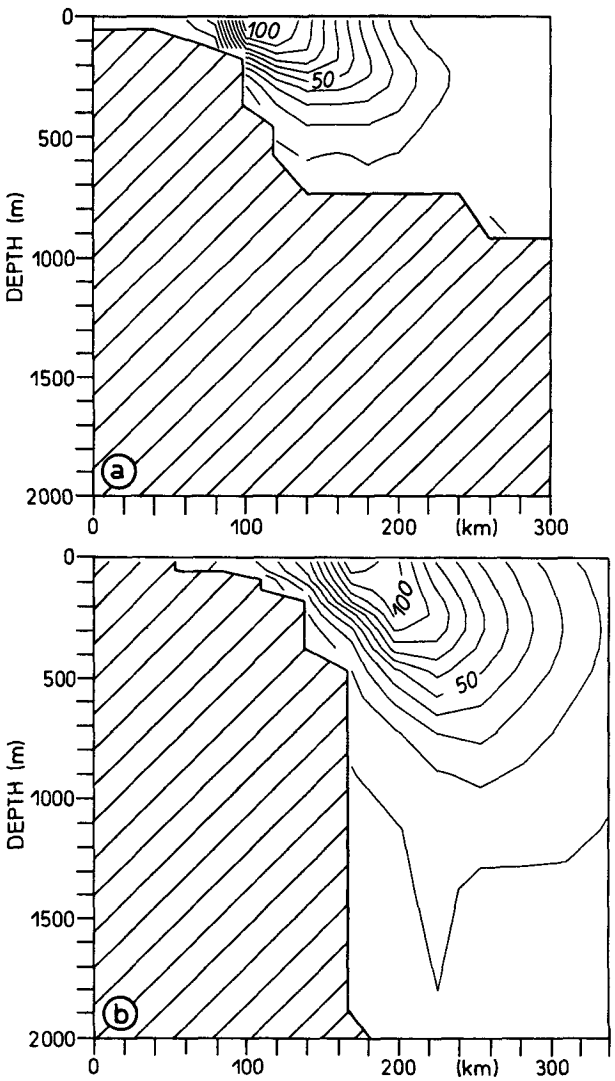

FIG. 13. Cross-jet sections through the boundary current (a) alongcoast average between 26° and 30°N and (b) alongcoast average between 32° and 35°N. Contour interval: 10 cm s^{-1}.

spatial scales are twice larger than in observations, which leads to a current shear reduced by a factor of three in both the horizontal and vertical direction. These specific structural differences point to a possible cause of the nonseparation: the model Gulf Stream is most likely too linear for "inertial separation." In addition it is too barotropic. A consideration of boundary-layer width and damping time scales might serve as an explanation for the unchanged boundary current width for both horizontal resolutions: for the biharmonic friction used in the CME model, the boundary-layer widths are $L_{1/3} = 26$ km and $L_{1/6} = 19$ km, respectively—a scale that is not at all resolved by the corresponding horizontal grids. The damping time scales in the boundary current region are $T_{\text{lateral}} = 200$ days for $A = -0.5 \times 10^{11}$ m^4 s^{-1} and $T_{\text{bottom}} = 30$ days for $U = 7.5$ cm s^{-1}; that is, the boundary current region is dynamically dominated by bottom friction, which was not changed for this very high resolution run.

b. What is the structure of the anticyclonic cells?

First, it is important to note that the newly developed LCC, just like the CHC, is a truly stationary feature (with only relatively small time variations) and not just the time-mean expression of a fluctuating loop current with growing meanders and detaching eddies. A close examination of LCC and CHC show remarkable similarities (Fig. 14). Both cells are nearly symmetric (the asymmetry, being about 10% of the radius, is mainly related to the nonrecirculating flow at the western and northern flanks), extend down to the bottom with velocities of a few cm s^{-1} (there is no flow reversal in the vertical), and have a decreasing radius with depth. The radius (measured from the center to the middepth velocity maximum) of both anticyclones is about 100 km and both are obviously in close interaction with topography. These similarities are even more surprising since the hydrographic situation in both areas is very different. A typical Rossby radius of deformation is 48 (28) km for the area of LCC (CHC). Although the presence of the anticyclones alters the stratification to give a Rossby radius of 57 (37) km in the center of LCC (CHC), it is obviously not the stratification but rather the nonlinearity that determines the size of these structures.

Symmetric ring vortices in gradient balance ($[v^2/r] + f_0 v = [\partial p/\partial r]$) represent a special stationary solution of the *nonlinear* equations of motion on an f plane, independent of their strength. On the sphere, a westward drift is introduced due to the variation of the Coriolis parameter. This asymmetry leads to a slow evolution: changes of strength and shape, or a translation of the center of mass. The latter may be blocked by topography and coastal geometry, that is, a vorticity balance between β and the topographic interaction term [joint effect of baroclinicity and bottom relief (JEBAR)]. The two dominating anticyclones in the model show this balance in good approximation if the nonrecirculating flow along the western and northern edge is subtracted. There is a strong (5 m day^{-1}) topographically induced net upwelling in the northwestern half of the cells and a corresponding downwelling of similar strength in the southeast, which balances the opposite tendency introduced by the variable Coriolis parameter. It is therefore concluded that the large barotropic component of these cells is responsible for their stationary character.

The increase in basin-averaged kinetic energy (see Fig. 2) can be almost completely attributed to the striking increase in strength of the two cells. Although covering only 2% of the model's area, LCC and CHC combined contain 25% of the MKE: most of the additional energy in the higher-resolution case available from reduced friction is "stored" in the anticyclones. They constitute a very special and robust circulation pattern that is resistant and absorbent relative to most perturbation energy.

The reason for this unrealistic CME model behavior, first mentioned by Bryan and Holland (1989), has ever since been a matter of speculation. [It should be emphasized that these structures are not a problem of the specific model used here; they can be found in many simulations of the North Atlantic (e.g., Semtner and Chervin 1992; Thompson and Schmitz 1989).] In a kinetic energy analysis of the 1/3° model N13-2, Treguier (1992) lists several possible causes for the deficiencies of the model vis-a-vis too low levels of eddy kinetic energy, one being the existence of the CHC. The other arguments concern model resolution, mixed-layer parameterization, numerical formulation, missing Mediterranean Water influence, and frictional parameters, some of which also apply here.

- The existence of the stationary anticyclones could be caused by the interplay between local bottom topography and stratification; although 1/6° is currently the best achievable resolution for a North Atlantic–wide simulation, it is certainly far from adequately resolving processes such as topographic shelf waves, details of wind-induced upwelling, and locally generated equatorward undercurrents at the western boundary. Regional models, especially designed for simulating processes along the continental shelves, usually require a resolution of less than 10 km. Therefore it seems possible that even higher horizontal (and, in addition, vertical) resolution might reduce and, finally, eliminate these structures.
- Another class of possible causes is that parameterizations are suboptimal for some regions. In particular, one could certainly give reasons for choosing different coefficients for lateral, vertical, and bottom friction in the shelf area off the North American East Coast. At present, however, both an increase and a decrease of these coefficients could be argued for (a question that is, in fact, under debate in the modeling com-

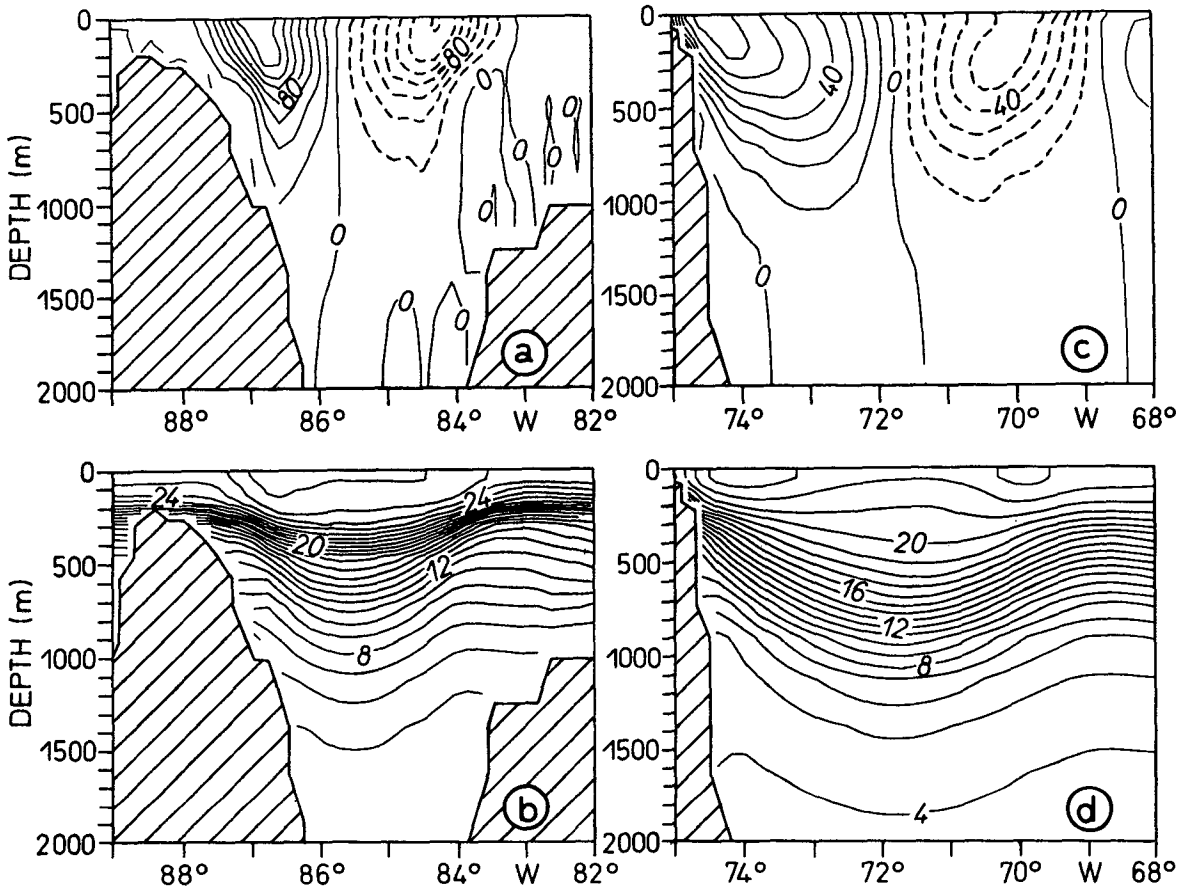

FIG. 14. Upper-ocean vertical structure of the anticyclonic cells in the Gulf of Mexico at 23°N (LCC: a,b) and at Cape Hatteras at 37°N (CHC; c,d). Sections through the anticyclone's center of (a), (c) the meridional velocity field (contour interval: 20 cm s^{-1} and 10 cm s^{-1}, respectively) and (b), (d) the temperature field (contour interval: 1°C).

munity). A reduction of friction will certainly lead to more nonlinearity, thus favoring an advective regime that could sweep the stationary cells away (see Dengg 1993), while more friction near the wall and the bottom is expected to move the axis of the core of the WBC offshore and thus to reduce the interaction with the topography. Also, the most appropriate form of the dissipative operators (Laplacian, biharmonic) in the model and the corresponding boundary conditions are open questions, too.

• One obvious reason for the unrealistically strong barotropic nature of most model flows might be a misrepresentation of the deep thermohaline structure and circulation in the model, which allows the surface structures to extend further down than in reality. Deficiencies of the climatological initial and forcing data as well as the artificial boundary conditions (in the northern and southern sponge layers) could be assumed responsible.

• Local deficiencies in the forcing fields (unrealistic wind and/or thermohaline forcing) could be [and have been, see Ezer and Mellor (1992)] made responsible for incorrect circulation over the shelf. While this might seem plausible for the CHC region, it is less likely that similar mechanisms can be made responsible for the Loop Current region in the Gulf of Mexico.

• The similarities in structure and scale of both anticyclonic cells despite their different geographical and dynamical environment could be interpreted as an indication of a "numerical" origin. Potentially problematic is the nonequidistant vertical grid, which can introduce additional vertical diffusion (Yin and Fung 1991) and thus contribute to a more barotropic flow field. The time-mean vertical velocity creates a numerical vertical diffusion of $\kappa_{num} = \pm 10^{-3}$ m^2 s^{-1}, thus reaching and exceeding the explicitly prescribed values of $\kappa_M = 10^{-3}$ m^2 s^{-1} for momentum and $\kappa_T = 3 \times 10^{-5}$ m^2 s^{-1} for tracers. Instantaneous values are higher by a factor of 5 to 10. In addition, the treatment of topography and the formulation of the advection operators (see Gerdes et al. 1991) are not fully investigated for spurious effects on model results. Likewise, the orientation of the grid with respect to major frontal features, and the aspect ratio of horizontal grid boxes might also influence the quality of a simulation.

Supporting evidence for the idea that deficiencies in the vertical structure and the thermohaline circulation may cause the unrealistic Gulf Stream separation comes from a series of runs with wind-driven dynamics only. For these sensitivity studies, the CME model code is used in a vertically integrated version, keeping the same geometry and numerical representation, but eliminating all thermodynamics and assuming a flat bottom at 1000-m depth (roughly coinciding with the basin-averaged thermocline depth). Variation of the coefficients for biharmonic viscosity, bottom friction, Laplacian friction, the strength of forcing and the formulation of the advection operator show only little effect on the western boundary current structure and the separation pattern; a more or less intense anticyclone in the Mid-Atlantic Bight persists through all parameter changes. If the full three-dimensional CME model behaves qualitatively like this simplified and purely wind-driven two-dimensional, it seems likely that an underrepresentation of the thermohaline circulation in the CME models may cause the lack of realism in connection with the boundary current separation. This, however, cannot easily explain the existence of the LCC.

7. Summary and discussion

The lack of numerical resolution has long been considered to be one of the major limiting factors in basin-scale numerical modeling, especially with primitive equation models. With today's computer resources it is possible to perform basinwide (CME) and worldwide (Semtner and Chervin 1992) "eddy-resolving" calculations. Common to all these approaches, however, are certain deficiencies in the representation of important phenomena. The first systematic approach, the CME, is characterized by several unrealistic features (Bryan and Holland 1989; Treguier 1992), in connection with the boundary current separation, the short penetration scale of the NAC, and the nonexistence of the ACFZ and the low overall level of EKE. It was repeatedly speculated (and hoped) that increasing resolution would increase the fluctuating component of the flow considerably and at the same time cure both the boundary current separation and the penetration deficiencies of the model. Unfortunately, the latter could not be confirmed with this increased horizontal resolution experiment; even the opposite could be regarded as being true for certain aspects of the mean circulation.

This paper has concentrated on an (admittedly incomplete) description of the time-mean circulation and its variability in a $1/6° \times 1/5°$ North Atlantic model. In general, as effects of the higher resolution on the mean hydrographic fields are small (which seems plausible, since the time scales needed for such changes are generally much longer than the present calculation was carried out), the increased resolution of this model version tends to confirm results from the $1/3°$ run; that is, there is no fundamentally different behavior. The horizontal velocities are only slightly higher, fronts tend to be a little sharper, and the mean circulation is only moderately more energetic. With a few exceptions, these being the strength of the anticyclonic cells along the western boundary, no dramatic changes in time-mean patterns have developed. This is in part surprising (after all, the highly energetic scales are represented twice as well compared to the $1/3°$ runs), but also reassuring in that a lot can be learned from further studies with the $1/3°$ model. On the other hand, the present run clearly demonstrates that very high horizontal resolution is a prerequisite if a realistic representation of the ocean's variability in a numerical model is to be obtained. And although the observed values are still not reached in this $1/6°$ resolution model, the increase in EKE as compared to the $1/3°$ is substantial.

The previously noted (and so far unexplained) trend toward smaller values of the mean meridional overturning with increased resolution continues. The net heat transport, however, remains almost unaffected by this reduced overturning, because the eddy-induced drop in mean transport constitutes a compensation for the eddy transport. Unfortunately, this precludes definitive statements about the relative importance of eddy versus mean transport of heat in the ocean. The resulting range of values for these integral quantities is indicative of how moderate changes in wind climatology, mixed layer, and subgrid-scale parameterization influence the model results, and, given the present knowledge of how these parameters and forcing functions have to be specified appropriately, of the reduced conclusiveness from single simulation experiments.

At this stage in global-scale modeling, the strategy should be to systematically eliminate these uncertainties in parameterization, forcing, boundary conditions, etc. Investigations of the influence of the boundary conditions in the northern restoring zone are currently under way for a coarse resolution (1°) version of this model (Döscher et al. 1993). They indicate a relatively fast and far-reaching response to changes in the θ–S distribution along the (artificial) northern wall. Analogous results were obtained by R. Gerdes (1992, personal communication), who also modified the water mass properties in the Denmark Strait to be significantly different from Levitus. One effect of a more realistic (denser) water in the overflow region noted in these studies is a Gulf Stream that is shifted toward the south (away from the North American coast) by a few degrees. Future experiments should consider the following modifications:

1) an improved treatment of the Arctic overflow and Mediterranean Water masses to obtain a more realistic circulation of the middepth and deep ocean, either by inclusion of an inflow–outflow boundary condition, or by a more effective parameterization, which

mimics the salt and temperature flux into the North Atlantic in a more realistic way;

2) a different (horizontally varying) lateral friction, to further reduce the diffusion in the poleward areas of the model; and

3) higher vertical resolution and/or a more uniform vertical grid (possibly in combination with a depth dependent vertical viscosity) to improve the representation of the vertical structure.

Acknowledgments. The 1/6° simulation was supported by the Bundesministerium für Forschung und Technologie (BMFT) under Grant 07 KFT 45. The calculations reported herein were conducted on the CRAY-2 at the German Climate Research Center (DKRZ) in Hamburg. The 1/3° experiments were performed as part of the Sonderforschungsbereich 133, financed by the Deutsche Forschungsgemeinschaft (DFG). Special thanks are due Peter Herrmann, Joachim Dengg, Reinhard Budich, and Ralf Döscher for their continuous assistance.

REFERENCES

Anderson, D. L. T., and R. A. Corry, 1985: Seasonal transport variation in the Florida Straits: A model study. *J. Phys. Oceanogr.*, **15,** 773–786.

Beckmann, A., C. W. Böning, B. Brügge, and D. Stammer, 1993: Generation and role of eddy variability in the central North Atlantic Ocean: *J. Geophys. Res.*, submitted.

Böning, C. W., and R. G. Budich, 1992: Eddy dynamics in a primitive equation model: Sensitivity to horizontal resolution and friction. *J. Phys. Oceanogr.*, **22,** 361–381.

——, and P. Herrmann, 1994: Annual cycle of poleward heat transport in the ocean: Results from high resolution modeling of the North and equatorial Atlantic. *J. Phys. Oceanogr.*, **24,** 91–107.

——, R. Döscher, and R. G. Budich, 1991a: Seasonal transport variation in the western subtropical North Atlantic: Experiments with an eddy-resolving model. *J. Phys. Oceanogr.*, **21,** 1271–1289.

——, ——, and H.-J. Isemer, 1991b: Monthly mean wind stress and Sverdrup transports in the North Atlantic: A comparison of the Hellerman–Rosenstein and Isemer–Hasse climatologies. *J. Phys. Oceanogr.*, **21,** 221–239.

Brügge, B., and J. Dengg, 1991: Differences in drift behavior between drogued and undrogued satellite-tracked drifting buoys. *J. Geophys. Res.*, **96,** 7249–7263.

Bryan, K., 1986: Poleward buoyancy transport in the ocean and mesoscale eddies. *J. Phys. Oceanogr.*, **16,** 927–933.

——, 1991: Poleward heat transport in the ocean. *Tellus,* **43AB,** 104–115.

——, and W. R. Holland, 1989: A high resolution simulation of the wind and thermohaline-driven circulation in the North Atlantic ocean. *Parameterization of Small-Scale Processes. Proceedings Aha Huliko'a Hawaiian Winter Workshop.* P. Muller and D. Anderson, Eds., Honolulu, University of Hawaii, 99–115.

Camp, N. T., and R. L. Elsberry, 1978: Oceanic thermal response to strong atmospheric forcing, II. The role of one-dimensional processes. *J. Phys. Oceanogr.*, **8,** 215–224.

Cox, M. D., 1985: An eddy-resolving numerical model of the ventilated thermocline. *J. Phys. Oceanogr.*, **15,** 1312–1324.

——, 1987: An eddy-resolving numerical model of the ventilated thermocline. Time dependence. *J. Phys. Oceanogr.*, **17,** 1044–1056.

Dengg, J., 1993: The problem of Gulf Stream separation: A barotropic approach. *J. Phys. Oceanogr.*, **23,** 2182–2100.

Didden, N., and F. Schott, 1992: Seasonal variations in the western tropical Atlantic: Surface circulation from Geosat altimetry and WOCE model results. *J. Geophys. Res.*, **97,** 3529–3542.

Döscher, R., C. W. Böning, and P. Herrmann, 1993: Response of meridional overturning and heat transport in the North Atlantic to changes in thermohaline forcing in northern latitudes: A model study. *J. Phys. Oceanogr.*, **23,** submitted.

Drijfhout, S. S., 1994: Heat transport by mesoscale eddies in an ocean circulation model. *J. Phys. Oceanogr.*, **24,** 353–369.

Ezer, T., and G. L. Mellor, 1992: A numerical study of the variability and the separation of the Gulf Stream, induced by surface atmospheric forcing and lateral boundary flows. *J. Phys. Oceanogr.*, **22,** 660–682.

Gerdes, R., C. Köberle, and J. Willebrand, 1991: The role of numerical advection schemes in general circulation models. *Climate Dyn.*, **5,** 211–226.

Greenberg, D. A., and B. D. Petrie, 1988: The mean barotropic circulation on the Newfoundland shelf and slope. *J. Geophys. Res.*, **93,** 15 541–15 550.

Hall, M. M., and M. L. Bryden, 1982: Direct estimates and mechanisms of ocean heat transport. *Deep-Sea Res.*, **29,** 339–360.

Han, Y.-J., 1984: A numerical world ocean general circulation model. Part II: A baroclinic experiment. *Dyn. Atmos. Oceans,* **8,** 141–172.

Hellerman, S., and M. Rosenstein, 1983: Normal monthly wind stress over the world ocean with error estimates. *J. Phys. Oceanogr.*, **13,** 1093–1104.

Isemer, H. J., and L. Hasse, 1987: The Bunker climate atlas of the North Atlantic Ocean. Vol. 2, *Air–Sea Interactions,* Springer Verlag, 256 pp.

Krauss, W., 1986: The North Atlantic Current. *J. Geophys. Res.*, **91,** 5061–5074.

——, and R. H. Käse, 1984: Mean circulation and eddy kinetic energy in the eastern North Atlantic. *J. Geophys. Res.*, **89,** 3407–3415.

Leaman, K. D., E. Johns, and T. Rossby, 1989: The average distribution of volume transport and potential vorticity with temperature at three sections across the Gulf Stream. *J. Phys. Oceanogr.*, **19,** 36–51.

Levitus, S., 1982: *Climatological Atlas of the World Ocean.* NOAA Prof. Paper 13, U.S. Govt. Printing Office, 173 pp.

Olson, D., F. Schott, R. Zantopp, and K. Leaman, 1984: The mean circulation east of the Bahamas as determined from a recent measurement program and historical XBT data. *J. Phys. Oceanogr.*, **14,** 1470–1487.

Roemmich, D., and C. Wunsch, 1985: Two transatlantic sections: Meridional circulation and heat flux in the subtropical North Atlantic Ocean. *Deep-Sea Res.*, **32,** 619–664.

Sarmiento, J. L., 1986: On the North and Tropical Atlantic heat balance. *J. Geophys. Res.*, **91,** 11 677–11 689.

Schmitz, W. J., Jr., and W. S. Richardson, 1991: On the sources of the Florida Current. *Deep-Sea Res.*, **38**(Suppl. 1), 379–409.

Schott, F. A., and C. W. Böning, 1991: The WOCE model in the western equatorial Atlantic: Upper layer circulation. *J. Geophys. Res.*, **96,** 6993–7004.

——, T. N. Lee, and R. Zantopp, 1988: Variability of structure and transports of the Florida Current in the period range from days to seasonal. *J. Phys. Oceanogr.*, **18,** 1209–1230.

Semtner, A. J., and R. M. Chervin, 1992: Ocean general circulation from a global eddy-resolving model. *J. Geophys. Res.*, **97,** 5493–5550.

Spall, M. A., 1990: Circulation in the Canary Basin: A model/data analysis. *J. Geophys. Res.*, **95,** 9611–9628.

——, 1992: Rossby wave radiation in the Cape Verde Frontal Zone. *J. Phys. Oceanogr.*, **22,** 796–807.

——, 1993: A mechanism for low frequency variability and salt flux in the Mediterranean Salt Tongue. *J. Phys. Oceanogr.*, **23,** submitted.

Stammer, D., and C. W. Böning, 1992: Mesoscale variability in the Atlantic Ocean from Geosat altimetry and WOCE high resolution numerical modeling. *J. Phys. Oceanogr.*, **22,** 732–752.

Thompson, J. D., and W. J. Schmitz, Jr., 1989: A limited-area model of the Gulf-Stream: Design, initial experiments, and model-data intercomparison. *J. Phys. Oceanogr.*, **19,** 791–814.

Treguier, A. M., 1992: Kinetic energy analysis of an eddy resolving, primitive equation model of the North Atlantic. *J. Geophys. Res.*, **97,** 687–701.

Yin, F. L., and I. Y. Fung, 1991: Net diffusivity in ocean general circulation models with nonuniform grids. *J. Geophys. Res.*, **96,** 10 773–10 776.